DANISH METEOROLOGICAL INSTITUTE

SCIENTIFIC REPORT

02-03

Contribution of the
Danish Meteorological Institute
to the final report of
SAMMOA

CEC contract EVK2-1999-00315:
Spring-to-Autumn Measurements and Modelling
of Ozone and Active species

Bjørn M. Knudsen, Signe B. Andersen and Allan Gross

COPENHAGEN 2002

Contribution of the
Danish Meteorological Institute
to the final report of SAMMOA

CEC contract EVK2-1999-00315:
Spring-to-Autumn Measurements and Modelling
of Ozone and Active species

Bjørn M. Knudsen, Signe B. Andersen and Allan Gross

Scientific Report 02-16

ISBN: 87-7478-454-4
ISSN: 0905-3263
ISSN: 1399-1949 (Online)

Danish Meteorological Institute
Ministry of Transport
Lyngbyvej 100
DK-2100 Copenhagen
Denmark

Phone: +45 39 15 75 00
Fax: +45 39 27 10 80
www.dmi.dk

Contribution of the Danish Meteorological Institute to the final report of SAMMOA

CEC contract EVK2-1999-00315: Spring-to-Autumn Measurements and Modelling of Ozone and Active species.

Bjørn M. Knudsen, Signe B. Andersen, Allan Gross

Main conclusions

1. At least 26% of the observed downward trend in ozone at northern mid-latitudes in May 1979-97 is caused by export of ozone depletion from the polar vortex. For 1995 and 1997 it has previously been found that about 40% of the observed depletion originates from the vortex.

2. The export of ozone depletion from the polar vortex together with circulation changes explain 80% of the longitudinal variations in mid-latitude ozone trends in April and May1979-97. This helps explain why the mid-latitude downward ozone trends are largest over Europe and Russia. Any increase in ozone depletion in the polar vortex as a result of future cooling of the stratosphere would therefore be particularly bad for Europe and Russia.

WP3. Dilution and ozone depletion in the spring

Activity 3.2. Mid-latitude depletion in spring

Chipperfield and Jones (1999) argue that most of the variation in Arctic (63º-90ºN) total ozone in March from 1992 to 1997 is dominated by dynamical variations. We have used the best available published estimated of the vortex depletions to derive its influence on the Arctic total ozone in March (Andersen and Knudsen, 2002), and find that vortex ozone depletion and transport effects are equally important for the ozone variations. Moreover, we find that vortex depletions account for 75% of the decrease from 1979-82 to 1992-2000.

Activity 3.3. Northern mid-latitude ozone dilution in spring.

It has long been known that trends in the circulation can explain a substantial fraction of the longitudinal ozone trend differences in winter. Entzian and Peters [2000] showed that trends in the 300 hPa geopotential height from 1979-1992 explains around half the longitudinal trend differences from 1979-1992 all the year round. Observations by the TOMS instrument onboard the Nimbus-7, Meteor 3, and Earth Probe satellites from 1979-1997 have shown that the largest spring ozone depletions over the northern and southern midlatitudes occur over Europe and Russia [WMO, 1999], except for large depletions south of 55°S. We have updated the circulation trends to 1997 and they still explain about half the longitudinal trend differences in April and May. They do, however, not explain the strong April and May trends over Scandinavia and especially Russia, but when including the transport of ozone depleted air from the vortex it almost does.

In this study Northern Hemisphere ozone depletions originating from the winter/spring vortex in 1995 and 1997 have been taken from Knudsen and Grooβ [2000]. They were calculated by following the depleted air with reverse domain-filling (RDF) trajectory calculations covering the altitude region of the ozone depletion (350-550K potential temperature (θ) or approximately 13-22 km height). Diabatic descent was calculated by the Morcrette radiation scheme. The ozone depletion mixing ratios were regridded every 7th day to introduce nearly realistic mixing on average Knudsen and Grooβ [2000]. These calculations might be termed RRDF (regridded RDF) calculations. The resulting average column depletion for April and May is shown in Figure 1. Part of the depletion results in an irreversible dilution of the midlatitude ozone. The calculations in Knudsen and Grooβ [2000] started on April 11th, so the vortex depletions on April 4th were added here. Also the calculations were corrected for the isentropic differences in depletion inside the vortex as shown by Knudsen et al. [1998].

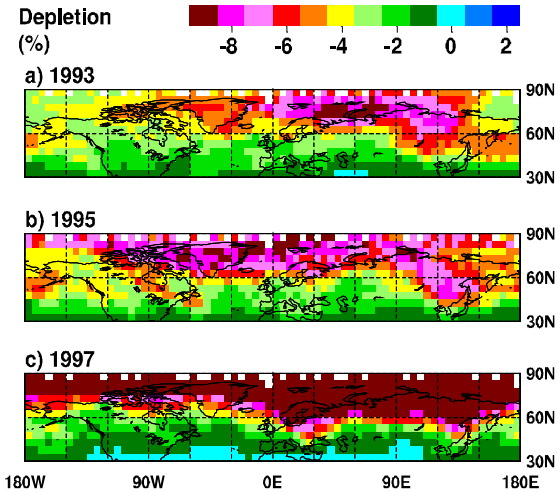

Figure 1. April-May averages of the depletion originating from the polar vortex in 1993 (a), 1995 (b) and 1997 (c). 5° latitude-longitude boxes were used.

In 1993 Larsen et al. [1994] used ozone soundings from Greenland to calculate the vortex ozone depletion. From their article it is evident that most of the ozone depletion has occurred by March 5th. Therefore we have determined the depletion as the difference between the vortex ozone soundings from Scoresbysund on March 5th and January 13th (corrected for diabatic descent). While this is not generally a feasible approach the results of Larsen et al. [1994] indicate that it is in 1993 since the variations in ozone mixing ratio inside the vortex were small that year. March 5th was chosen as the end date because the size of the vortex decreased substantially thereafter. As a zero order approximation the effect of the diffusive transport into the vortex was taken from 1997 calculations [Knudsen et al., 1998]. The vortex average column depletion from 375 – 525 K is 79 DU. Of these 24 DU are below 400 K and therefore possibly below the vortex, where the calculated depletions are most uncertain because e.g. the diffusive transport is biggest. The depletions at 375 and 400 K seem to agree quite well with the results of Müller et al. [1996], however. Figure 1a shows the depletion originating from the vortex in 1993.

By picking the years 1993 and 1997 we have included the major part of the vortex depletion, since the TOMS column ozone data used here have a gap from December 1994 to July 1996 and also in May 1994 [McPeters et al., 1996]. Braathen et al. [2000] have shown that at 475 K the depletion in the winters 1991/1992 and 1988/1989 was small, and only in the winter

1989/1990 ozone depletions comparable to the depletion in 1993 were found. In the winter 1990/1991 little PSC activation was predicted [Pawson et al., 1995], so little ozone depletion is expected. In earlier winters the depletion potential is considerably reduced due to smaller amounts of chlorine and bromine.

Simple linear regression results in the trends given in Figure 2a. Like Entzian and Peters [2000] we did not take the influence of e.g. the quasibiennual oscillation (QBO) into account. This should, however, not have a great influence since the time series is so long. The March to May trends are slightly larger [WMO, 1999] because the largest depletion occurs in March. The April and May period is, however, most interesting biologically due to increased exposure to harmful ultraviolet radiation.

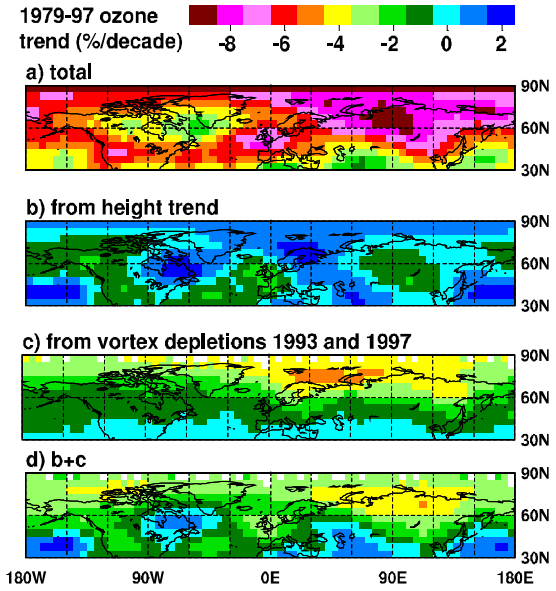

Figure 2. (a) The April-May 1979-97 ozone trend. (b) The ozone trend due to the trend in the 250 hPa height. (c) The ozone trend due to the vortex depletions in 1993 and 1997. (D) The sum of b and c.

Trends in the height of the 250 hPa geopotential from 1979-97 were calculated exactly as the ozone trends using ECWMF analyses. In order to calculate the effect of trends in the planetary wave structure on trends in ozone, regression and correlation coefficients for the spatial distribution of ozone and the 250 hPa geopotential were calculated. To avoid interference from chemical ozone depletion this was done for the period 1979-1984. A regression coefficient of 0.16 DU/gpm was found for the April-May average at 30° - 60°N in good agreement with the 300 hPa results for 1979-92 in Entzian and Peters [2000].

Figure 2b shows the trend in ozone that may be explained by the trend in the 250 hPa geopotential. This trend was obtained by multiplying the trend in the 250 hPa geopotential with the regression coefficient mentioned above. It is clear that the height trend does a good job explaining that the downward ozone trend is weak south of Greenland and strong over the UK. But it does not explain the strong trends over e.g. Scandinavia and Russia.

The effect of the transport of ozone depleted air from the polar vortex in 1993 and 1997 on the observed ozone trends is calculated in the following way: The 1993 and 1997 depletion (as shown in Figure 1) is added to the observed ozone in the same years. The ozone trend for

this data set is then calculated and subtracted from the ozone trend shown in Figure 2a. The resulting trend shown in Figure 2c helps explain the strong downward ozone trends over Scandinavia and Russia. By neglecting the vortex depletion in other years than 1993 and 1997 the effect of the vortex depletion will be underestimated. The part of the midlatitude (30°-60°N) trend that may be attributed to the vortex depletion amounts to 0.7%/decade or 18% of the observed ozone trend on average (DE3.4). This might be compared to the 25% of the observed ozone depletion in only April and May 1997, which was found to originate from the vortex depletion [Knudsen and Grooβ, 2000]. For May alone the part of the midlatitude trend that may be attributed to the vortex depletion amounts 26% of the observed ozone trend (DE3.4). For May 1995 and 1997 Knudsen and Grooβ [2000] found that about 40% of the observed depletion originated from the vortex. The discrepancy could be due to the neglect of ozone depletion in other years than 1993 and 1997.

In Figure 2d the trends in panels b and c in Figure 2 have been added and the combination does explain quite a fraction of the longitudinal trend variations. From 30°-60°N it explains 60% of the variation (the correlation is 0.77), whereas the height trend alone only explains 41% for the April to May period. Using a multiple regression Knudsen and Andersen [2001] found that 80% of the midlatitude variation is explained. In April (May) alone the combined trend explains 66% (76%) of the variation, whereas the height trend only explains 49% (68%). The fact that the trends in panel a generally are more negative (~4%/decade) than the trends in panel d is due to e.g. local ozone depletion outside the vortex.

In the Southern Hemisphere the vortex is much more circumpolar and breaks up about two months later than in the Northern Hemisphere. Therefore the Antarctic vortex depletion has only little influence on the southern mid-latitudes in spring and this helps explain why the ozone downward trend in the northern midlatitudes is much stronger than in the southern in spring [WMO, 1999].

We have thus shown that the large vortex ozone depletions seen in the later years contribute to the observed spring ozone depletion over Europe and Russia mainly. Eastern Russia is at the climatological maximum of ozone, so the depletions here might not matter as much as the depletions over Europe, which is at the climatological minimum (longitudinally).

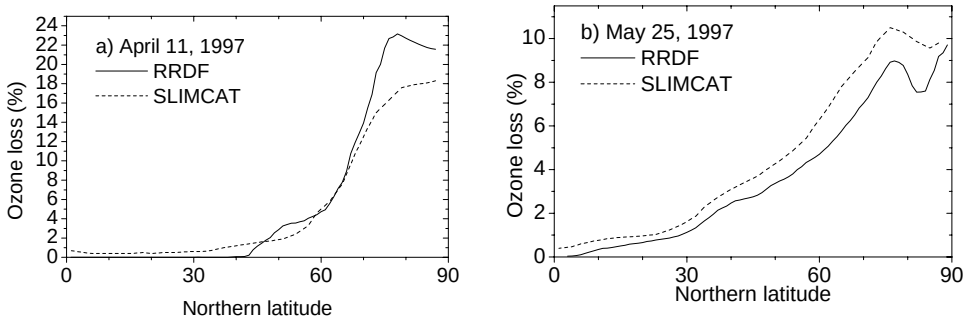

Figure 3. RRDF and SLIMCAT ozone loss compared on April 11 and May 25, 1997.

The RRDF calculations, which simply advect the end-of-winter vortex depletions, have been compared to the ozone loss tracer in the high-resolution SLIMCAT run with simplified PSC scheme and Cariolle ozone. Figure 3a shows the result for April 11, 1997 (April 10 for SLIMCAT). It is evident that SLIMCAT underestimates the vortex depletion, as it is common in cold winters. In SLIMCAT there is some depletion outside the vortex due to in-situ chemis-

try or export of vortex air prior to April 11. In figure 3b, the result for May 25, 1997, is shown. The increase in the SLIMCAT ozone loss compared to the DMI loss is probably due to the Cariolle scheme. In fact the total NH ozone loss from SLIMCAT increases 9% during the period, whereas it is expected to recover. The RRDF and SLIMCAT curves have approximately the same slope indicating that the mixing to lower latitudes is about the same (as expected from WP5.3).

WP4. Summer ozone loss over the Arctic and impact on mid-latitudes.

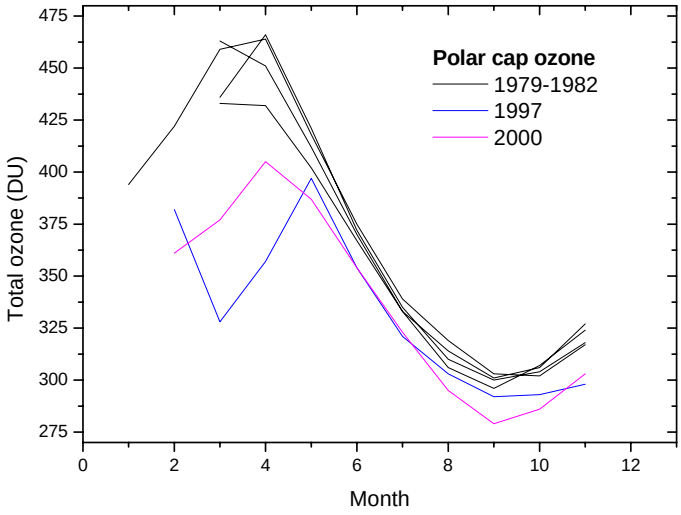

Figure 4: Monthly mean 60º-90ºN total ozone from TOMS.

In figure 4 the year-round development of the total ozone in the polar cap is shown. These data have been averaged in 10º bins (e.g. 80º-90ºN) and then the area-weighted average in the polar cap is formed. The North Pole is only sunlit from March 21 to September 21, so data from September to March should be used with caution. The plots shows the large ozone depletions in spring, but also show a rapid recovery from the depletion. At least by June the polar cap ozone seems to have recovered to an amount of depletion which persists throughout the whole summer, and which could be due to ongoing enhanced summer ozone loss due to man-made compounds. In the polar cap the recovery is presumably particularly fast due to rapid photochemistry in eternal sunlight, and the recovery at mid-latitudes is expected to be slower.

5.3. Effective mixing in regridded RDF calculations.

As mentioned in WP5.1 it is not possible to quantify the mixing in the model as originally proposed, by looking at tracer-tracer correlations. Instead the mixing is simulated. In the horizontal the diffusivity of the model is 1650 m^2s^{-1} [Knudsen and Grooß, 2000]. The vertical spacing is 25 K or about 1 km. With an aspect ration of 250 this corresponds to a horizontal distance of 250 km. Thus the linear interpolation in the vertical introduces the same mixing as a horizontal grid of 250 km spacing. This mixing is a factor of 5 larger than the horizontal mixing in the model (at 111 km grid resolution). The diffusivity of the model is therefore about $8.25 \cdot 10^3$ m^2s^{-1} instead of $1.65 \cdot 10^3$ m^2s^{-1}, or somewhat higher than the real diffusivity (which is less than 10^3 m^2s^{-1}. That means that the midlatitude dilution in WP 3.3 might be overestimated by about 2% [Knudsen and Grooß, 2000].

How does the mixing in the regridded RDF calculations compare to the mixing in a CTM as the SLIMCAT model? The SLIMCAT model uses the Prather [1986] advection scheme, which has a low diffusivity. On the other hand the timestep is only 15 minutes, which tends to increase the mixing. In figure 5 the mixing of a step function in the regridded RDF model is followed.

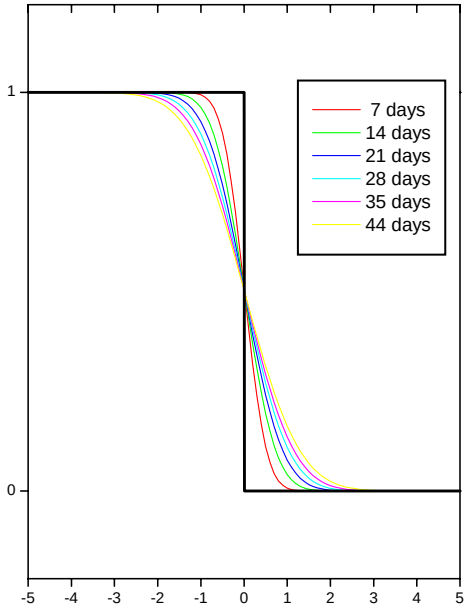

Figure 5. mixing of a step function with the regridded RDF model.

The units on the x-axis is grid-intervals, whereas the unit on the y-axis is arbitrary. This figure can be compared to figure 3a in Prather [1986]. Advection through 200 grid intervals (without limits) gives almost the same mixing as in the RDF model during 21 days. 200 grid intercals corresponds to 1000 time steps or about 10 days. That means for the same horizontal resolution the Prather scheme with a timestep of 15 minutes is slightly more diffusive (a factor of 2.1) than the RDF model. The diffusivity of the SLIMCAT model at 111 km grid spacing is thus $3.4 \cdot 10^3$ m^2s^{-1}, and at 555 km grid spacing the diffusivity is $9.0 \cdot 10^4$ m^2s^{-1}. Again the mixing in the vertical might be more important. SLIMCAT is often run at 3 km vertical spacing and with Prather advection in the vertical. For an aspect ratio of 250 this would lead to a diffusivity of $1.6 \cdot 10^5$ m^2s^{-1}.

References

Andersen, S. B., and B. M. Knudsen, The influence of vortex ozone depletion on Arctic ozone trends, *Geophys. Res. Lett.*, accepted 2002.

Braathen, G. O., et al., Temporal evolution of ozone in the Arctic vortex from 1988-89 to 1999-2000, paper presented at the SOLVE-THESEO 2000 Science Meeting, Palermo, 25-29 Sept., 2000.

Chipperfield, M. P., and R. L. Jones, Relative influences of atmospheric chemistry and transport on Arctic ozone trends, *Nature*, 551-554, 1999

Entzian, G. and D. Peters, Seasonal longitude dependent total ozone variations induced by large scale wave structure of the geopotential field over the northern hemisphere, Proc. Quadrennial Ozone Symposium, Sapporo, 3-8 July 2000.

Knudsen, B. M., and J.-U. Grooβ, Northern midlatitude stratospheric ozone dilution in spring modeled with simulated mixing, *J. Geophys. Res., 105*, 6885-6890, 2000.

Knudsen, B. M., and S. B. Andersen, Longitudinal variation in springtime ozone trends, *Nature, 413*, 699-700, 2001.

Knudsen, B. M., et al., Ozone depletion in and below the Arctic vortex for 1997, *Geophys. Res. Lett., 25*, 627-630, 1998

Larsen, N., B. Knudsen, I. S. Mikkelsen, T. S. Jørgensen, and P. Eriksen, Ozone depletion in the arctic stratosphere in early 1993, *Geophys. Res. Lett., 21*, 1611-1614, 1994.

McPeters, R. D., S. M. Hollandsworth, L.E. Flynn, J. R. Herman, and C. J. Seftor, Long-term ozone trends derived from the 16-year combined Nimbus 7/Meteor 3 TOMS Version 7 record, *Geophys. Res. Lett., 23*, 3699-3702, 1996.

Müller, R., P. J. Crutzen, J.-U. Grooβ, C. Brühl, J. M. Russell III, and A. F. Tuck, *J. Geophys. Res., 101*, 12,531-12554, 1996.

Pawson, S., B. Naujokat, and K. Labitzke, On the PSC formation potential of the northern stratosphere, *J. Geophys. Res., 100*, 23,215-23,225, 1995.

Prather, M. J., Numerical advection by conservation of second-order moments, *J. Geophys. Res., 91*, 6671-6681, 1986.

World Meteorological Organization (WMO), Scientific assessment of ozone depletion: 1998, *Global Ozone Res. Monitor. Proj. Rep. 44*, Geneva, 1999.

DANISH METEOROLOGICAL INSTITUTE

Scientific Reports

Scientific reports from the Danish Meteorological Institute cover a variety of geophysical fields, i.e. meteorology (including climatology), oceanography subjects on air and sea pollution, geomagnetism, solar-terrestrial physics, and physics of the middle and upper atmosphere.

Reports in the series within the last five years:

No. 97-1
E. Friis Christensen og C. Skøtt: Contributions from the International Science Team. The Ørsted Mission - a pre-launch compendium

No. 97-2
Alix Rasmussen, Sissi Kiilsholm, Jens Havskov Sørensen, Ib Steen Mikkelsen: Analysis of tropospheric ozone measurements in Greenland: Contract No. EV5V-CT93-0318 (DG 12 DTEE):
DMI's contribution to CEC Final Report Arctic Trophospheric Ozone Chemistry ARCTOC

No. 97-3
Peter Thejll: A search for effects of external events on terrestrial atmospheric pressure: cosmic rays

No. 97-4
Peter Thejll: A search for effects of external events on terrestrial atmospheric pressure: sector boundary crossings

No. 97-5
Knud Lassen: Twentieth century retreat of sea-ice in the Greenland Sea

No. 98-1
Niels Woetman Nielsen, Bjarne Amstrup, Jess U. Jørgensen: HIRLAM 2.5 parallel tests at DMI: sensitivity to type of schemes for turbulence, moist processes and advection

No. 98-2
Per Høeg, Georg Bergeton Larsen, Hans-Henrik Benzon, Stig Syndergaard, Mette Dahl Mortensen: The GPSOS project
Algorithm functional design and analysis of ionosphere, stratosphere and troposphere observations

No. 98-3
Mette Dahl Mortensen, Per Høeg: Satellite atmosphere profiling retrieval in a nonlinear troposphere.
Previously entitled: Limitations induced by Multipath

No. 98-4
Mette Dahl Mortensen, Per Høeg: Resolution properties in atmospheric profiling with GPS

No. 98-5
R.S. Gill and M. K. Rosengren: Evaluation of the Radarsat imagery for the operational mapping of sea ice around Greenland in 1997

No. 98-6
R.S. Gill, H.H. Valeur, P. Nielsen and K.Q. Hansen: Using ERS SAR images in the operational mapping of sea ice in the Greenland waters: final report for ESA-ESRIN's: pilot projekt no. PP2.PP2.DK2 and 2nd announcement of opportunity for the exploitation of ERS data projekt No. AO2..DK 102

No. 98-7
Per Høeg et al.: GPS Atmosphere profiling methods and error assessments

No. 98-8
H. Svensmark, N. Woetmann Nielsen and A.M. Sempreviva: Large scale soft and hard turbulent states of the atmosphere

No. 98-9
Philippe Lopez, Eigil Kaas and Annette Guldberg: The full particle-in-cell advection scheme in spherical geometry

No. 98-10
H. Svensmark: Influence of cosmic rays on earth's climate

No. 98-11
Peter Thejll and Henrik Svensmark: Notes on the method of normalized multivariate regression

No. 98-12
K. Lassen: Extent of sea ice in the Greenland Sea 1877-1997: an extension of DMI Scientific Report 97-5

No. 98-13
Niels Larsen, Alberto Adriani and Guido DiDonfrancesco: Microphysical analysis of polar stratospheric clouds observed by lidar at McMurdo, Antarctica

No.98-14
Mette Dahl Mortensen: The back-propagation method for inversion of radio occultation data

No. 98-15
Xiang-Yu Huang: Variational analysis using spatial filters

No. 99-1
Henrik Feddersen: Project on prediction of climate variations on seasonel to interannual timescales (PROVOST) EU contract ENVA4-CT95-0109: DMI contribution to the final report:Statistical analysis and post-processing of uncoupled PROVOST simulations

No. 99-2
Wilhelm May: A time-slice experiment with the ECHAM4 A-GCM at high resolution: the experimental design and the assessment of climate change as compared to a greenhouse gas experiment with ECHAM4/OPYC at low resolution

No. 99-3
Niels Larsen et al.: European stratospheric monitoring stations in the Artic II: CEC Environment and Climate Programme Contract ENV4-CT95-0136. DMI Contributions to the project

No. 99-4
Alexander Baklanov: Parameterisation of the deposition processes and radioactive decay: a review and some preliminary results with the DERMA model

No. 99-5
Mette Dahl Mortensen: Non-linear high resolution inversion of radio occultation data

No. 99-6
Stig Syndergaard: Retrieval analysis and methodologies in atmospheric limb sounding using the GNSS radio occultation technique

No. 99-7
Jun She, Jacob Woge Nielsen: Operational wave forecasts over the Baltic and North Sea

No. 99-8
Henrik Feddersen: Monthly temperature forecasts for Denmark - statistical or dynamical?

No. 99-9
P. Thejll, K. Lassen: Solar forcing of the Northern hemisphere air temperature: new data

No. 99-10
Torben Stockflet Jørgensen, Aksel Walløe Hansen: Comment on "Variation of cosmic ray flux and global coverage - a missing link in solar-climate relationships" by Henrik Svensmark and Eigil Friis-Christensen

No. 99-11
Mette Dahl Meincke: Inversion methods for atmospheric profiling with GPS occultations

No. 99-12
Hans-Henrik Benzon; Laust Olsen; Per Høeg: Simulations of current density measurements with a Faraday Current Meter and a magnetometer

No. 00-01
Per Høeg; G. Leppelmeier: ACE - Atmosphere Climate Experiment

No. 00-02
Per Høeg: FACE-IT: Field-Aligned Current Experiment in the Ionosphere and Thermosphere

No. 00-03
Allan Gross: Surface ozone and tropospheric chemistry with applications to regional air quality modeling. PhD thesis

No. 00-04
Henrik Vedel: Conversion of WGS84 geometric heights to NWP model HIRLAM geopotential heights

No. 00-05
Jérôme Chenevez: Advection experiments with DMI-Hirlam-Tracer

No. 00-06
Niels Larsen: Polar stratospheric clouds microphysical and optical models

No. 00-07
Alix Rasmussen: "Uncertainty of meteorological parameters from DMI-HIRLAM"

No. 00-08
A.L. Morozova: Solar activity and Earth's weather. Effect of the forced atmospheric transparency changes on the troposphere temperature profile studied with atmospheric models

No. 00-09
Niels Larsen, Bjørn M. Knudsen, Michael Gauss, Giovanni Pitari: Effects from high-speed civil traffic aircraft emissions on polar stratospheric clouds

No. 00-10
Søren Andersen: Evaluation of SSM/I sea ice algorithms for use in the SAF on ocean and sea ice, July 2000

No. 00-11
Claus Petersen, Niels Woetmann Nielsen: Diagnosis of visibility in DMI-HIRLAM

No. 00-12
Erik Buch: A monograph on the physical oceanography of the Greenland waters

No. 00-13
M. Steffensen: Stability indices as indicators of lightning and thunder

No. 00-14
Bjarne Amstrup, Kristian S. Mogensen, Xiang-Yu Huang: Use of GPS observations in an optimum interpolation based data assimilation system

No. 00-15
Mads Hvid Nielsen: Dynamisk beskrivelse og hydrografisk klassifikation af den jyske kyststrøm

No. 00-16
Kristian S. Mogensen, Jess U. Jørgensen, Bjarne Amstrup, Xiaohua Yang and Xiang-Yu Huang: Towards an operational implementation of HIRLAM 3D-VAR at DMI

No. 00-17
Sattler, Kai; Huang, Xiang-Yu: Structure function characteristics for 2 meter temperature and relative humidity in different horizontal resolutions

No. 00-18
Niels Larsen, Ib Steen Mikkelsen, Bjørn M. Knudsen m.fl.: In-situ analysis of aerosols and gases in the polar stratosphere. A contribution to THESEO. Environment and climate research programme. Contract no. ENV4-CT97-0523. Final report

No. 00-19
Amstrup, Bjarne: EUCOS observing system experiments with the DMI HIRLAM optimum interpolation analysis and forecasting system

No. 01-01
V.O. Papitashvili, L.I. Gromova, V.A. Popov and O. Rasmussen: Northern polar cap magnetic activity index PCN: Effective area, universal time, seasonal, and solar cycle variations

No. 01-02
M.E. Gorbunov: Radioholographic methods for processing radio occultation data in multipath regions

No. 01-03
Niels Woetmann Nielsen; Claus Petersen: Calculation of wind gusts in DMI-HIRLAM

No. 01-04
Vladimir Penenko; Alexander Baklanov: Methods of sensitivity theory and inverse modeling for estimation of source parameter and risk/vulnerability areas

No. 01-05
Sergej Zilitinkevich; Alexander Baklanov; Jutta Rost; Ann-Sofi Smedman, Vasiliy Lykosov and Pierluigi Calanca: Diagnostic and prognostic equations for the depth of the stably stratified Ekman boundary layer

No. 01-06
Bjarne Amstrup: Impact of ATOVS AMSU-A radiance data in the DMI-HIRLAM 3D-Var analysis and forecasting system

No. 01-07
Sergej Zilitinkevich; Alexander Baklanov: Calculation of the height of stable boundary layers in operational models

No. 01-08
Vibeke Huess: Sea level variations in the North Sea – from tide gauges, altimetry and modelling

No. 01-09
Alexander Baklanov and Alexander Mahura: Atmospheric transport pathways, vulnerability and possible accidental consequences from nuclear risk sites: methodology for probabilistic atmospheric studies

No. 02-01
Bent Hansen Sass and Claus Petersen:
Short range atmospheric forecasts using a nudging procedure to combine analyses of cloud and precipitation with a numerical forecast model

No. 02-02
Erik Buch: Present oceanographic conditions in Greenland waters